JOURNAL OF SOLID STATE CHEMISTRY **128,** 42–51 (1997)
ARTICLE NO. SC967145

"Chimie Douce" Synthesis and ab Initio Structure Determination of $(H_3O)Yb_3F_{10},H_2O$: A Diamond Type Stacking of $UOA_{[8]}$

J-J. Maguer, M. P. Crosnier-Lopez, and G. Courbion[1]

Laboratoire des Fluorures, URA CNRS 449, Faculté des Sciences, Université du Maine, 72017 Le Mans Cedex, France

Received April 15, 1996; in revised form September 9, 1996; accepted September 10, 1996

The fluoride $(H_3O)Yb_3F_{10},H_2O$ (SG: $Fd\bar{3}m$, $a=15.326(1)$ Å, $Z=16$) was synthesized in the form of powder by a "chimie douce" route. The compound δ-KYb_3F_{10},H_2O (SG: $Fd\bar{3}m$, $a=15.339(1)$ Å, $Z=16$), a new member of the KYb_3F_{10} family, was obtained by an acid–base neutralization. The structural description is based upon the stacking of $[Yb_6F_{32}]^{14-}$ "octahedral units of antiprism," called $UOA_{[8]}$, where the three-dimensional $[Yb_6F_{20}]^{2-}$ network is simply a diamond type stacking of $UOA_{[8]}$ connected by vertices. The counterions are located in the middle of the chair hexagons. The zeolithic character of the water molecules is related to their mobility through the tunnels of this diamond structure. The simplifying description of this phase as a diamond type structure built up from $UOA_{[8]}$ ($A_2[Yb_6F_{20}],2H_2O$, $A=H_3O^+$, $Z=8$) is the basis of our reexamination of the structural description of numerous complex structures built up of antiprisms. © 1997 Academic Press

INTRODUCTION

Numerous fluorinated compounds involving lanthanide elements and alkaline metals, or alkaline earth metals, are known. This is not the case for fluorides in which 3d transition cations are associated with 4f rare earth ions. To our knowledge, only the $MnLuF_5$ compound (1) and the $NaLnCu_2F_8$ family (2) are reported. For the former compound, no structural study has been reported, but for the $NaLnCu_2F_8$ series (Ln = Eu, Gd, Yb) the structure is claimed to be isotypic with the $KBrF_4$ type. Our first aim was to prepare new fluorinated compounds with 4f and 3d elements, due to their potential magnetic properties. As all of our attempts in the solid state were unsuccessful, we decided to experiment with a "chimie douce route" via lanthanide and 3d oxalate precursors. During these trials, performed mainly with M = Mn and Ln = Yb, we found only the title compound. The present scope of this paper is to report the synthesis, the characterization, and the structure determination of $(H_3O)Yb_3F_{10},H_2O$.

[1] To whom correspondence should be addressed.

SYNTHESIS

A "chimie douce" process allowed for the synthesis of $(H_3O)Yb_3F_{10},H_2O$. In a first step, an amount of Yb_2O_3 was dissolved in a minimum amount of boiling nitric acid. An oxalic acid solution was then added to this solution so that a hydrated $Yb_2(C_2O_4)_3,xH_2O$ precipitate was obtained, then filtered out, washed with water, and air dried. In a second step, this salt was added to a heated solution of HF 49% in order to synthesize the fluoride. The most efficient temperature which yielded the best crystallinity of the resulting product $(H_3O)Yb_3F_{10},H_2O$ was empirically found to be 70°C. Our compound was obtained in the form of a fine white powder with no single crystal included.

SPACE GROUP DETERMINATION

X-ray powder patterns used for the structural determination were recorded on a Philips PW1380 goniometer equipped with a back graphite monochromator. Indexing of the first 25 reflections of the powder pattern was obtained utilizing the program TREOR (3), in a cubic system, with $a = 15.322(1)$ Å. This solution was characterized by the following figures of merit: $M(25) = 32$, $F(25) = 35$. Then, 72 reflections were indexed up to large angle with the cell parameter refined by the program ERACEL (4) remaining unchanged at 15.327(1) Å. The hkl observed reflections lead to the c.f.c. lattice. The highest symmetry space group $Fd\bar{3}m$ (no. 227, origin choice 2 at center $\bar{3}m$) was deduced from the following conditions: $hk0: h + k = 4n$ and $h, k = 2n$; $hhl: h + l = 2n$; $h00: h = 4n$.

CHARACTERIZATION

The fluorine analysis confirmed that the ionic network was made up completely of fluoride, as the mean experimental percentage, 25.5(7)% (2 measures), was in agreement with the 25.46% theoretical value for $(H_3O)Yb_3F_{10},H_2O$. One can notice that if an anionic site had been occupied by OH^- instead of F^-, i.e., a 32e site (see crystallographic

0022-4596/97 $25.00

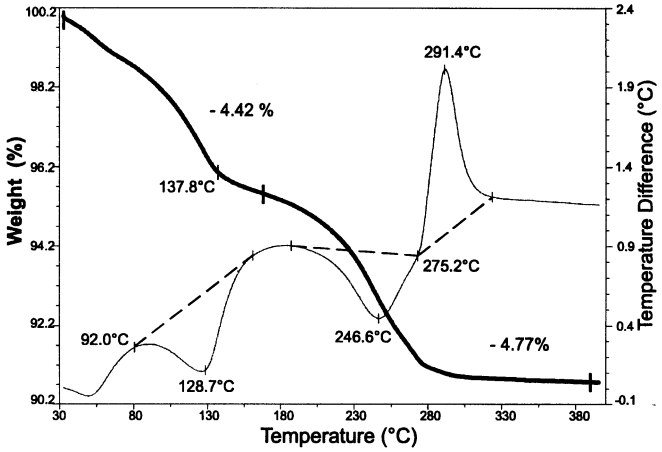

FIG. 1. DTA/TGA curves for $(H_3O)Yb_3F_{10},H_2O$.

data), the fluorine percentage for $(H_3O)Yb_3F_8(OH)_2,H_2O$ should have been much lower (20.48%).

Numerous data were collected from DTA (T.A. Instruments SDT 2960) and TGA (Setaram TGA 92 12) experiments. The coupled thermogravimetric and thermal analysis data collected at 400°C are shown in Fig. 1. It clearly exhibits a two-step loss of matter associated with three thermal phenomena. The first two peaks, both below 260°C, correspond to a loss of water without destruction of the crystalline building. The third exothermic peak between 275 and 330°C corresponds to the decomposition of the starting compound to YbF_3 with a loss of HF. These observations have been verified by X-ray thermodiffractometry analysis, shown in Fig. 2. The decomposition begins at 240 and ends at 360°C (the temperature difference between the thermodiffractometric and thermogravimetric techniques is approximately 20°C).

The first endothermic peak is correlated to a loss of weight which corresponds to zeolithic water. This phenomenon has been observed in a thermogravimetric study by which we heated our compound to a temperature of 130°C and then slowly cooled it to room temperature. It has been shown in a first analysis under argon that the loss of weight due to the heating was stabilized upon cooling. For the same experiment under air, we observed an increase of weight upon cooling, corresponding to a reabsorption of water (see Fig. 3).

A quantitative analysis of our thermal studies is critical. The main objective is to determine the true amount of absorbed water due to time-dependent natural desorption. The total weight loss before decomposition reached 9.19% for a freshly synthesized sample (see Fig. 1). Two days later, the weight loss decreased to 8.02%. Finally, after a few weeks under atmospheric conditions, the observed loss was only 7.60%. The first two weight loss values indicated 1.5 to 2 H_2O per formula. The last value is close to the theoretical weight loss for $(H_3O)Yb_3F_{10},H_2O$ (7.51%) and corresponds to the stabilized water content which exhibits a zeolithic character. Indeed, as can be seen in Fig. 3, the weight increase (0.73 mg) when cooled under air corresponds to

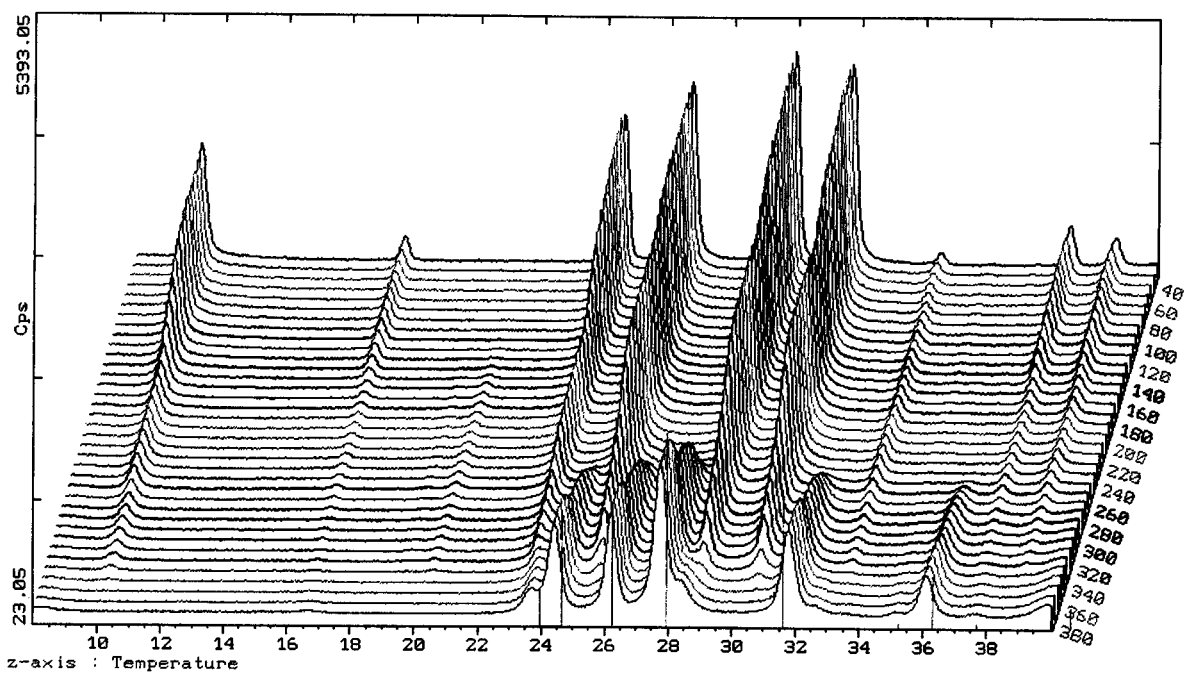

FIG. 2. X-ray thermodiffraction of $(H_3O)Yb_3F_{10},H_2O$ (vertical bars are related to YbF_3).

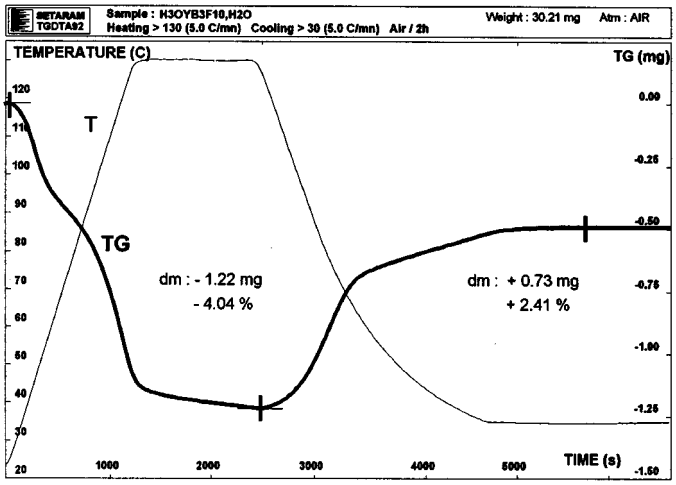

FIG. 3. TGA experiment under air for $(H_3O)Yb_3F_{10},H_2O$.

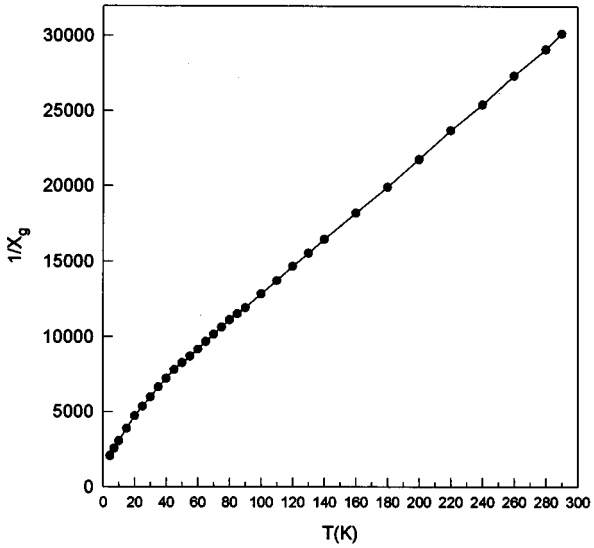

FIG. 4. $\chi^{-1} = f(T)$ curve for $(H_3O)Yb_3F_{10},H_2O$.

4.05×10^{-5} mol of reabsorbed H_2O. The mass of anhydrous fluoride, $(H_3O)Yb_3F_{10}$, at the end of the step was equal to 28.99 mg (30.21–1.22 mg), i.e., 3.98×10^{-5} mol. The ratio of zeolithic water is thus close to one.

From a qualitative point of view, we can retain that three steps appear during the thermal treatment:

(1) zeolithic water desorption

$$(H_3O)Yb_3F_{10},H_2O \rightarrow (H_3O)Yb_3F_{10} + H_2O$$

(2) elimination of H_2O associated to H_3O^+

$$(H_3O)Yb_3F_{10} \rightarrow \text{“}HYb_3F_{10}\text{”} + H_2O$$

(3) decomposition

$$HYb_3F_{10} \rightarrow HF + 3YbF_3.$$

Steps (2) and (3) are not separable on the thermogravimetric curve, which is in agreement with the X-ray thermodiffractograms that show the appearance of YbF_3 before the total disappearance of the starting compound. However, each step is distinguishable by TDA: (1) and (2) are endothermic phenomena, (3) is an exothermic decomposition.

DTA/TGA measurements show that the appearance of “HYb_3F_{10}” at the second step begins above 130°C. It is associated with the appearance of the low intensity 222 reflection at 120°C that is visible on the thermodiffractogram near 20° (2θ), and with a perceptible decrease of several intensities (for example: 111 reflection). Attempts to fit the 222 reflection from the “HYb_3F_{10}” composition were unsuccessful.

An infrared spectroscopy study also confirmed the presence of H_2O or H_3O^+ molecules: a weak but broad band at 1627 cm^{-1} and a very broad, intense band in the 3500-cm^{-1} region were observed.

Finally, susceptibility measurements were performed in the temperature range 4.2–300 K using a Faraday method ($H = 0.7$ T). The thermal variation of the reciprocal magnetic susceptibility (gram) is given in Fig. 4. A Curie–Weiss law is observed above 40 K. For the composition $(H_3O)Yb_3F_{10},H_2O$, the calculated Curie constant and the paramagnetic Curie temperature were $C_M = 8.26$, $\theta p = -42$ K, respectively. The effective moment per ytterbium ion, 4.69 μ_B, is then close to the theoretical 4.54 μ_B value for a Yb^{3+} ion ($S = 1/2$, $L = 3$, $J = L + S = 7/2$, $\mu_{theo} = g\sqrt{J(J+1)}$ with $g = 8/7$). Below 40 K, the slight deviation from linearity is probably the consequence of the zero-field splitting of the Yb^{3+} multiplet induced by the crystal field rather than the reflect of antiferromagnetic couplings.

AB INITIO X-RAY STRUCTURE DETERMINATION

A profile matching mode of the program FULLPROF (5) was used to calculate the intensities. The quality of the refinement was improved by suppressing the 111 strong reflection at 10.01°2θ, which was highly asymmetric. The fit of the 422 and 822 reflections remained incorrect, the calculated intensities being inferior to the observed data. From this refinement ($Rp = 11.9\%$, $Rwp = 14.4\%$, $\chi^2 = 30.2$, $R_B = 6.2\%$, $R_F = 3.7\%$), 196 intensities were converted into structure factors and used as input for the program SHELXS-86 (6). Scattering factors for Yb^{3+}, F^-, and O^{2-} were taken from the “International Tables for Crystallography” (7). The position of the heavy atom was located by using the option TREF, for 50 nonoverlapping reflections (at least 0.06°2θ apart).

A refinement of the atomic coordinates and of the thermal motion of a Yb^{3+} ion situated in a 48f site ($\frac{3}{8}$ $\frac{3}{8}$ 0.053),

yielded to an agreement factor of $R = 19.4\%$. The difference-Fourier map showed several peaks with distances to heavy atoms characteristic of Yb–F bond length. The reliability factor of successive atomic position and thermal motion refinements of F_1 (96*e*: 0 0.87–0.87), F_2 (32*e*: $x = 0.21$), and F_3 (32*e*: $x = 0.053$) decreased to 6.6%.

The deduced composition, $Yb_{48}F_{160}$, was not balanced as it corresponded to $[Yb_3F_{10}]^-$, with $Z = 16$. At this stage, the surrounding of the Yb^{3+} cation is well defined and corresponds to an almost regular antiprism YbF_8. The analysis of the difference-Fourier map allowed for the localization of an electronic density in the 16*d* ($\bar{3}m$) site. We assigned this density to an H_3O^+ molecule (formally, O^{2-}, hydrogen atom being not visible). This counterion ensures the charge balance of the deduced $(H_3O)Yb_3F_{10}$ formula. In the subsequent refinement, the thermal motion of the hydronium ion converged to 4.1 Å^2 and the reliability factor decreased to 5.6%. Furthermore, an electronic density situated in a 48*f* site ($\frac{3}{8}$ $\frac{3}{8}$ 0.20) could be seen on the difference-Fourier map. This peak could be explained by additional water molecules. The occupation ratio of an O^{2-} ion situated in this site decreased to a third of its initial value and was then exactly fixed to $\frac{1}{3}$. At this condition, its thermal motion drops to about 3 Å^2, and the reliability factor decreased to 5.0%. The final composition was then $(H_3O)Yb_3F_{10},H_2O$.

At this point, we went back to the Rietveld refinement of the powder diffractogram. This calculation allowed for a better refinement of the position of the water molecules: it converged to $\frac{3}{8}$ $\frac{3}{8}$ 0.245, which generated H_2O–F_1 distances of 2.66 Å, instead of a shorter 2.2 Å distance. A 422 preferred orientation can be used to lower the I_{obs}–I_{cal} difference for the 422 and 822 reflections, but the problem concerning these two profiles remains unsolved. The conventional reliability values of the last refinement are $Rp = 14.2\%$, $Rwp = 16.9\%$, $\chi^2 = 42.6$, $R_B = 7.6\%$, $R_F = 6.1\%$. The conditions of the powder data collection and refinement are reported on Table 1. The observed and calculated patterns

TABLE 1
Condition of Powder Data Recording (300 K) and Refinement for $(H_3O)Yb_3F_{10},H_2O$

Angular range (°2θ):	5–40		
Step (°2θ):	0.02		
Time/step (sec):	33		
Receiving slits (°):	0.1		
Refinement program:	FULLPROF		
Space group:	$Fd\bar{3}m$ (227)		
Cell parameters (Å):	$a = 15.326(1)$		
Volume (Å^3)/Z:	3599.9(7)/16		
Zero point: (°2θ):	0.0323		
Background:	selected by hand		
Number of reflections:	197		
Peak shape:	Thompson–Cox–Hastings pseudo-Voigt		
FWHM parameters:	$U_1 = 0.018(1)$	$V_1 = -0.024(2)$	$W_1 = 0.0101(7)$
Asymmetry parameters:	0.173(3)	0.051(1)	
Microstrain parameter:	$Y = 0.101(1)$		
Preferred orientation:	$G1 = 0.940(3)$ (March function)		
Number of parameters:	17		
Conventional reliability factors:	$Rp = 14.2\%$	$Rwp = 16.9\%$ $R_B = 7.56\%$	$\chi^2 = 42.6$ $Rf = 6.11\%$

Note. Data recorded using a Philips PW 1380 diffractometer, Cu$K\alpha$.

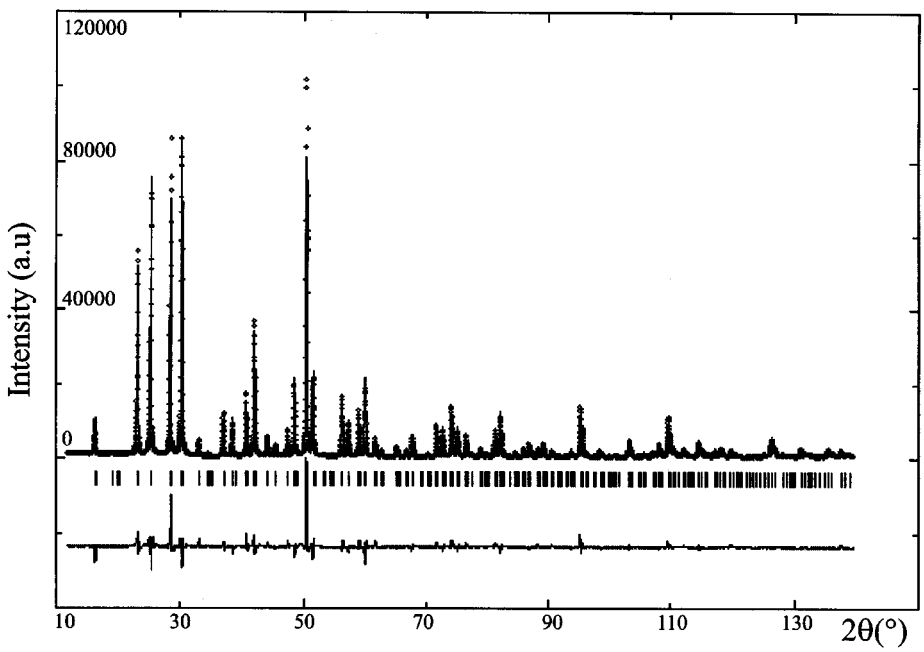

FIG. 5. Observed (···) and calculated (——) X-ray powder pattern of $(H_3O)Yb_3F_{10},H_2O$. The difference pattern is shown below at the same scale (vertical bars are related to the line's position).

TABLE 2
Atomic Parameters and Isotropic Beq Temperature Factors ($Å^2$) for $(H_3O)Yb_3F_{10},H_2O$ ($Fd\bar{3}m$, Origin: 16*c*)

Atom	Site	*x*	*y*	*z*	Beq
Yb	48*f*	$\frac{3}{8}$	$\frac{3}{8}$	0.0531(1)	0.59(1)
F_1	96*h*	0	0.8749(4)	− 0.8749(4)	0.29
F_2	32*e*	0.2118(4)	0.2118(4)	0.2118(4)	0.22*
F_3	32*e*	0.0538(4)	0.0538(4)	0.0538(4)	0.22*
H_3O^+	16*d*	$\frac{1}{2}$	$\frac{1}{2}$	$\frac{1}{2}$	3.7(7)
H_2O	48*f*[a]	$\frac{3}{8}$	$\frac{3}{8}$	0.245(2)	3.7*

[a] Occupation ratio $\frac{1}{3}$.
* denotes fixed factor.

are presented in Fig. 5. The atomic parameters and thermal motions are given on Table 2.

TEM ANALYSIS

An electron microscopy study confirmed the structure determination. An EDX analysis, performed with a JEOL-2010 TEM equipped with a KEVEX energy dispersive X-ray spectrometer, revealed crystals with the mean composition $Yb_3F_{10}O$. No impurity was detected. Cell parameters were found to be $a = b = c = 15.3(2)$ Å. The deduced reflection conditions:

— $hkl : h, k, l$ same parity (F lattice)
— $0kl : k + l = 4n$, and $k, l = 2n$ (d type plane)
— $00l : l = 4n$

lead to the following possible space groups: $Fd\bar{3}m$ (or $Fd\bar{3}$) and $Fd\bar{3}c$. A careful examination of the intensities showed the existence of a multiple diffraction phenomenon: it was found that the intensity of the hhl with $h + l = 2n$, but $h, l \neq 2n$ reflections was constant regardless of the tilt of the crystal. Thus, only the $hhl : h + l = 2n$ condition was perfectly confirmed. The $Fd\bar{3}c$ space group was then discarded. Finally, the deduced extinction symbol was $Fd-$ ($Fd\bar{3}m$ or $Fd\bar{3}$ space groups), which is in perfect agreement with the X-ray diffraction study.

Figure 6a shows an electron diffraction pattern of a twinned crystal. Such patterns have often been observed. By comparison to a pattern of a nontwinned crystal (Fig. 6b) with the same zone axis, the first pattern can be explained by the twinning of two crystals having the same [101] zone axis with a {111} twinning plane, the twinning angle being 109°5. The [111]* row is common to the two crystals, as well as the [101]* row which is parallel to the incident beam.

HREM images of a complete focal series could not be taken because of a fast deterioration of the crystal under the beam. A simulation has been performed with the help of the program EMS of Stadelman (8) by the multislice method. The agreement between the observed and calculated image (Fig. 7) is very good.

STRUCTURAL DESCRIPTION

The coordination polyhedron of the Yb^{3+} ion is a square antiprism involving eight F^- (see Fig. 8). The mean Yb–F distance, 2.25(1) Å, is in a good agreement with the theoretical distance (2.28 Å) for eight coordinated Yb^{3+} ions (Table 3). The maximum and minimum Yb–F distances ($2.211(6)$ Å $< d <$ $2.345(6)$ Å) are close to the observed extrema for β and γ-KYb_3F_{10} (β-KYb_3F_{10} (9): $2.108(5)$ Å $< d <$ 2.335 Å, $\langle d_{Yb-F}\rangle = 2.23$ Å; γ-KYb_3F_{10} (10): $2.199(5)$ Å $< d <$ 2.376 Å, $\langle d_{Yb-F}\rangle = 2.29$ Å). The square faces of the antiprism are of different dimensions, as

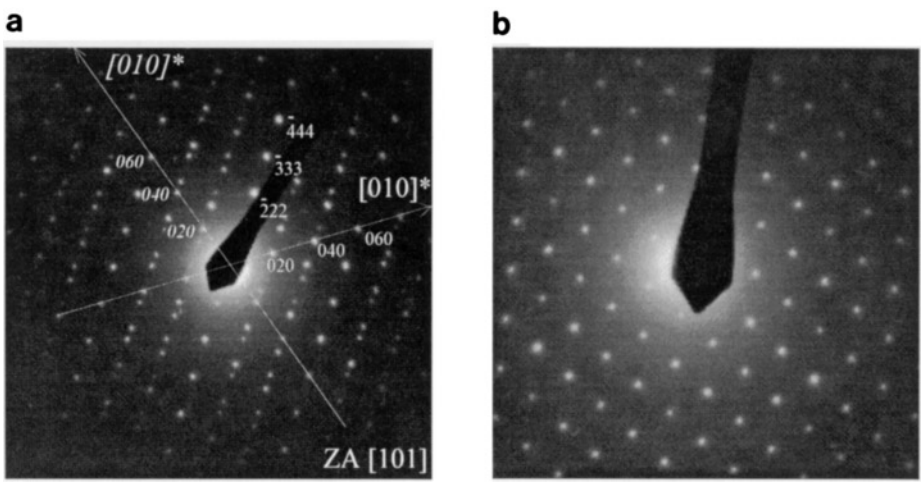

FIG. 6. Electron diffraction pattern for $(H_3O)Yb_3F_{10},H_2O$: (a) twinned crystal (b) nontwinned crystal.

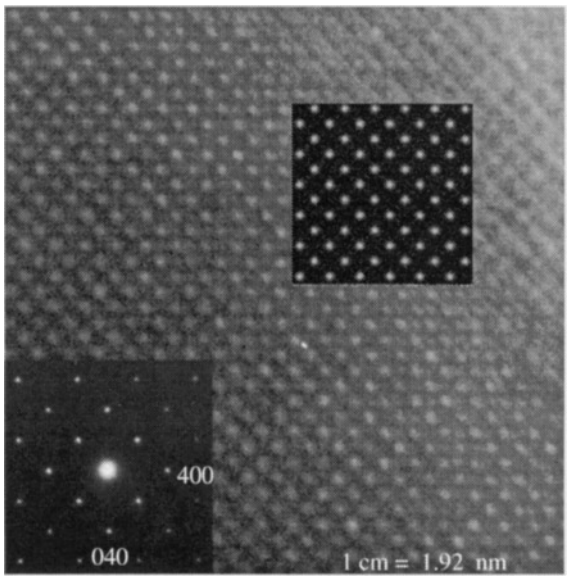

FIG. 7. Observed and simulated HREM images along the [001] zone axis.

is usually observed for rare earths in such a coordination: the square face made by the four F_1 anions exhibits F_1–F_1 distances (2.710(6) Å) greater than the F_2–F_3 distances (2.446(11) Å) observed for the square face made by the F_2 and F_3 anions. The Yb^{3+} ion is correlatively slightly off-center, being closer to the largest face: Yb–F_1 distances are shorter than Yb–F_2 and Yb–F_3 distances.

Each polyhedron shares the four F_2–F_3 edges of the smallest square face with four neighboring antiprisms. As can be seen in Fig. 9, six antiprisms are therefore connected around a distorted cubic cavity for which angles range between 78.3(6)° and 100.6(5)° instead of 90°. This forms an $[Yb_6F_{32}]^{14-}$ structural unit, which resembles the geometry of an octahedron. For this reason, as well as for clarity, this unit will be further called *octahedral unit of antiprisms*, noted by $UOA_{[8]}$. In this abbreviation, the index [8] is used for indicating the number of anions constituting the central cavity (cubic in this case).

TABLE 3
Main Distances (Å) in $(H_3O)Yb_3F_{10},H_2O$

Yb^{3+} polyhedron: [8]	F–F distances in the square antiprisms
$4\times Yb–F_1 : 2.211(6)$	$2\times F_1–F_1 = 2.709(6)$
$2\times Yb–F_3 : 2.251(6)$	$2\times F_1–F_1 = 2.710(6)$
$2\times Yb–F_2 : 2.345(6)$	$4\times F_1–F_2 = 2.892(7)$
$\langle d_{Yb-F}\rangle = 2.25(1)$ Å	$4\times F_1–F_3 = 3.063(10)$
$d_{Shannon} = 2.28$ Å	$4\times F_2–F_3 = 2.446(11)$
Center of the hexagonal cavity	
$6\times(H_3O^+)–F_1 : 2.709(7)$	
Zeolithic water	
$4\times(H_2O)–F_1 : 2.66(1)$	

Each free vertex of an octahedral unit of antiprisms is shared with another $UOA_{[8]}$. Moreover, two $UOA_{[8]}$ are linked by six vertices, noted, **a, b, c, d, e, f** in Fig. 9. Each $UOA_{[8]}$ is then linked to four neighboring $UOA_{[8]}$ tetrahedrally (see Fig. 10a). The formula of the resulting three-dimensional structure is then $[Yb_6F_{20}]^{2-}$: $Yb_6F_{32} \equiv Yb_6F_8F'_{24} \rightarrow Yb_6F_8F'_{24/2} \equiv Yb_6F_{20}$. As can be seen in Fig. 10b, in which each $UOA_{[8]}$ is symbolized by a sphere, the three-dimensional network of $(H_3O)Yb_3F_{10},H_2O$ can be described as a diamond type stacking of $UOA_{[8]}$ sharing vertices. The true formula is thus $(H_3O)_2Yb_6F_{20},2H_2O$, with $Z = 8$.

Tunnels along [110] directions (see Fig. 11), chair hexagons and cavities (see Fig. 12) are of course the main features of this noncompact diamond type stacking. The H_3O^+

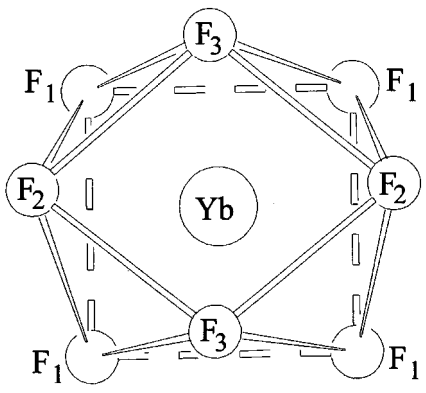

FIG. 8. Coordination polyhedron for Yb^{3+}.

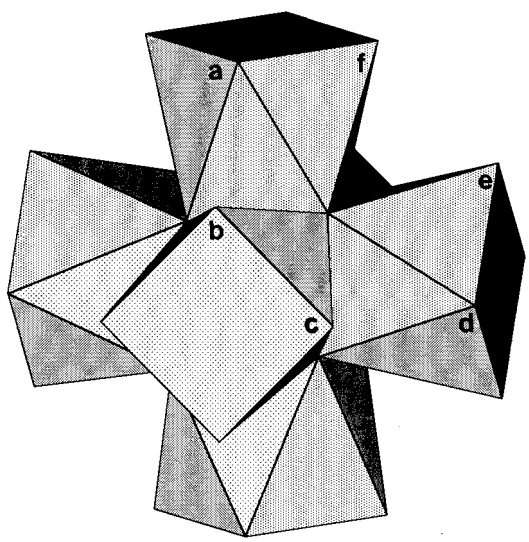

FIG. 9. $[Yb_6F_{32}]^{14-}$ structural unit: an $UOA_{[8]}$ whose empty central cavity is a cube.

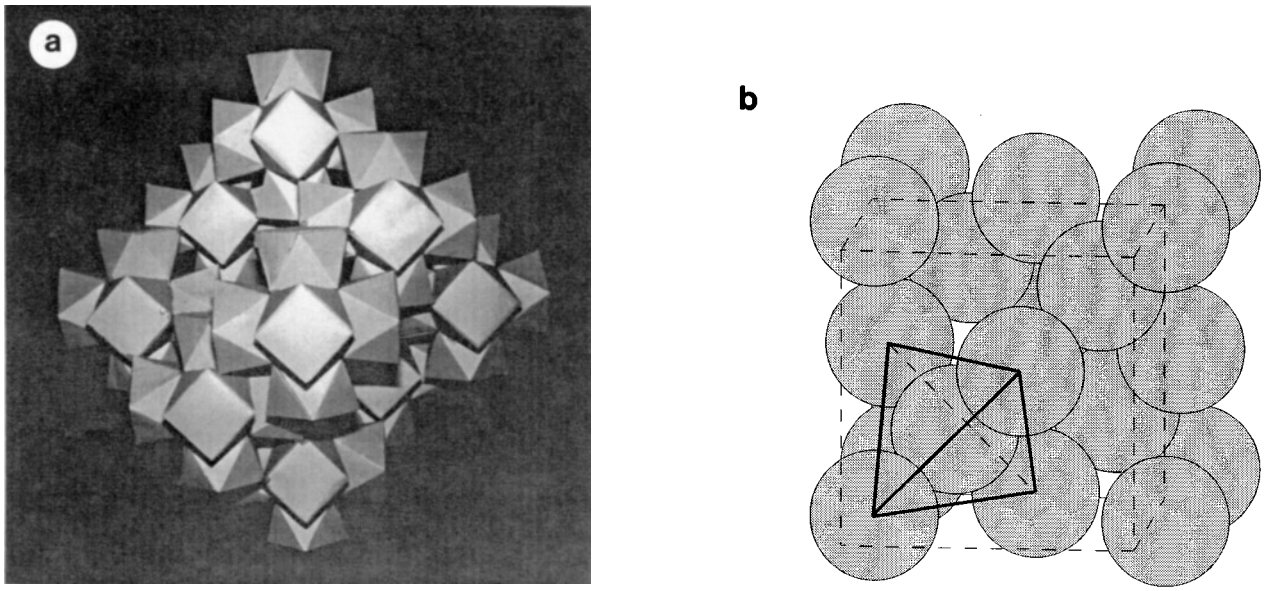

FIG. 10. (a) structure of $(H_3O)Yb_3F_{10},H_2O$ viewed along [100]: $[Yb_6F_{20}]^{2-}$ network (b) the same view with spheres instead of $UOA_{[8]}$.

cations are located in the middle of the chair hexagons [16*d* position), at the center of an open face of pseudo hexagonal symmetry, leading to six (H_3O)–F_1 distances equal to 2.709 Å. As can be seen in Fig. 13, the water molecules are statistically distributed inside the large cavities centered in the 8*b* position ($\frac{3}{8}\frac{3}{8}\frac{3}{8}$). These cavities are made of 28 F^-, the mean ((8*b* site)–F) distance being 4.29 Å (24*x* 4.284(6) Å + 4*x* 4.331(6) Å). The free radius of the sphere corresponding to this cage is 2.98 Å, its free volume being 111 $Å^3$. Four open faces of pseudo-hexagonal symmetry delimit this cage, each face being common to two cages.

Four (H_2O)–F_1 distances, 2.66(1) Å, are observed. (H_3O)–F_1 and (H_2O)–F_1 are thus in the range 2.56–2.86 Å quoted by Simonov and Butvesky (11) and characteristic for O–H ⋯ F hydrogen bonding in metal fluoride hydrates. Bond length analysis is also presented in Table 4. The F_1 anion exhibits the lowest valency, as it is linked by hydrogen bonding together to H_3O^+ and H_2O.

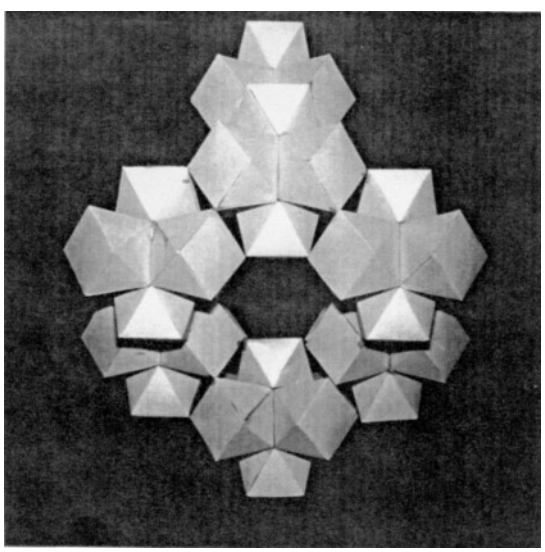

FIG. 11. $(H_3O)Yb_3F_{10},H_2O$: structure viewed along [110] showing tunnels.

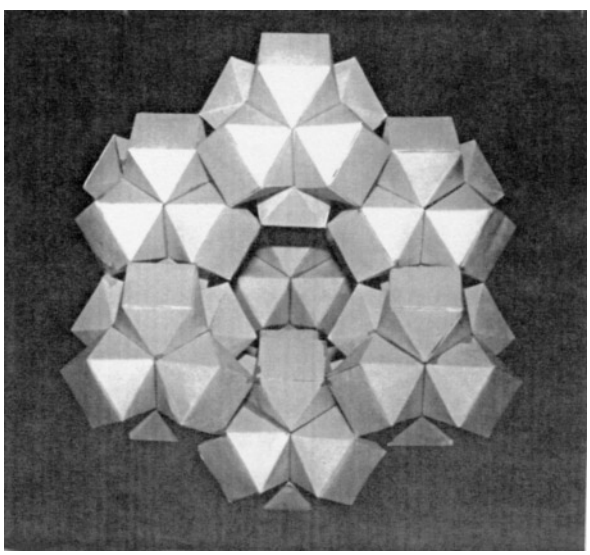

FIG. 12. $(H_3O)Yb_3F_{10},H_2O$: structure viewed along [111].

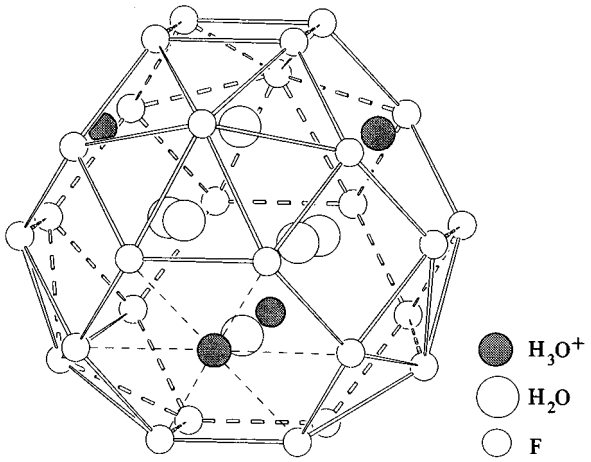

FIG. 13. Cage built up from the connection of 10 $UOA_{[8]}$. The open faces are occupied by H_3O^+ and the cavity, statistically, by zeolithic water molecules.

CATIONIC EXCHANGE AND SYNTHESIS OF δ-KYb_3F_{10},H_2O

The zeolithic properties of $(H_3O)Yb_3F_{10},H_2O$ have been clearly related to the structure of this compound which exhibits a three-dimensional network of tunnels. As the H_3O^+ cations are also situated in these tunnels, we thought it possible to replace them by an alkaline cation of equivalent radius. Since the H_3O^+ effective radius was 1.41 Å (2.709–1.30), we decided to make experiments with potassium ($r = 1.38$ Å in a sixfold coordination).

A first test of cationic exchange by mixing our fluoride with a solution of KF was unsuccessful. In a second trial, we tried to obtain a potassium precipitate by adding the starting oxalate salt to a heated HF/KF (5 *M*) solution. As a result, we synthesized a badly crystallized sample of cubic γ-(or α-)KYb_3F_{10} whose refined cell parameter was $a = 11.301(5)$ Å (*Note*: *the KYb_3F_{10} family exhibits three phases*: $\alpha - 769°C \rightarrow \beta$ (*hexagonal*) $- 952°C \rightarrow \gamma$ (*cubic*). *The α and γ forms have been reported to be isotypic* (10). *The $\alpha \rightarrow \beta$ transformation is not observable by DTA, but only by electric conductivity*). The thermal behavior of our compound, studied both by DTA and X-ray thermodiffraction techniques, was different from the observed behavior for the KYb_3F_{10} phases synthesized in the solid state at high temperature. Indeed, above 450°C, the compound partially decomposed to δ-KYb_2F_7, then above 750°C to YbOOH + δ-K_3YbF_6, and finally to Yb_2O_3 above 900°C.

At last, an acid–base neutralization was performed successfully at room temperature under stirring according to the reaction

$$(H_3O)Yb_3F_{10},H_2O + KOH(0.5\,M) \rightarrow KYb_3F_{10},H_2O + 2\,H_2O.$$

The resulting sample is a diamond type compound, K^+ replacing H_3O^+. In order to avoid confusion, this new phase has been called δ-KYb_3F_{10},H_2O.

The crystallographic analysis of this compound has been determined by powder X-ray diffraction. The cell parameter $a = 15.339(1)$ Å, is very close to that of $(H_3O)Yb_3F_{10},H_2O$. The conditions of data recording on a Siemens D500 diffractometer (Cu$K\alpha$) and refinement are reported on Table 5. The structure refinement of δ-KYb_3F_{10},H_2O has been performed by analogy with $(H_3O)Yb_3F_{10},H_2O$ (the only visible difference between these two diffractograms corresponds to the presence of the low but nonnegligible 222 reflection). The 111 reflection was also discarded because of a high asymmetry. Calculated intensities of the 422 and 822 reflections were inferior to the observed ones, as in the first case, but the I_{obs}–I_{cal} difference was far smaller. The conventional values of the last refinement are $R\text{p} = 11.2\%$, $R\text{wp} = 12.3\%$, $\chi^2 = 13.0$, $R_B = 6.99\%$, $R_F = 4.96\%$. The observed and calculated patterns are presented in Fig. 14. A refinement of the occupation ratio of the K^+ position proved that this site was fully occupied, as τ converged to 98%. It is also noticeable that the Rp or R_B values are about 5% greater when K^+ is replaced by H_3O^+ (formally O^{2-}).

TABLE 4
Bond Length Analysis in $(H_3O)Yb_3F_{10},H_2O$

Ions		$\sum s$	$\sum s_{th}$
Yb	$4\times0.407 + 2\times0.291 + 2\times0.368$	2.95	3
F_1	2×0.407	0.81	1
F_2	3×0.291	0.87	1
F_3	3×0.368	1.10	1

TABLE 5
Condition of Powder Data Recording (300 K) and Refinement for δ-KYb_3F_{10},H_2O

Angular range (°2θ):	7–127		
Step (°2θ):	0.03		
Time/step (sec):	13		
Receiving slits (°):	0.1		
Space group:	$Fd\bar{3}m$ (227)		
Cell parameters (Å):	$a = 15.339(1)$		
Volume (Å^3)/Z:	3609.0(7)/16		
Zero point: (°2θ):	0.0082		
Number of reflections:	173		
Peak shape:	Thompson–Cox–Hastings pseudo-Voigt		
FWHM parameters:	$U_1 = 0.036(1)$	$V_1 = -0.029(2)$	$W_1 = 0.0273(6)$
Asymmetry parameters:	0.112(4)	0.037(1)	
Number of parameters:	18		
Conventional reliability factors:	$R\text{p} = 11.2\%$	$R\text{wp} = 12.3\%$	$\chi^2 = 13.0$
		$R_B = 6.99\%$	$R\text{f} = 4.96\%$

Note. Data recorded using a Siemens D500 diffractometer, Cu$K\alpha$.

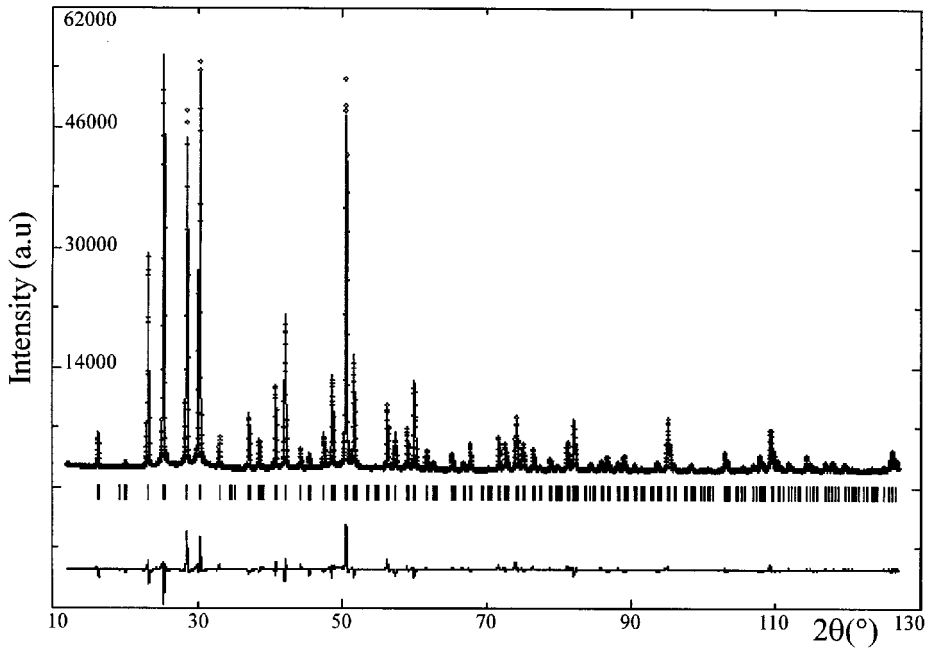

FIG. 14. Observed (···) and calculated (——) X-ray powder pattern of δ-KYb_3F_{10},H_2O. The difference pattern is shown below at the same scale.

Atomic parameters and thermal motions are given on Table 6. The interatomic distances (Table 7) are similar to those of $(H_3O)Yb_3F_{10},H_2O$.

The thermal behavior of δ-KYb_3F_{10},H_2O has been studied by TGA/DTA. The exothermic decomposition of this phase is observed between 429 and 455°C (peak maximum at 434°C). Above this temperature, the anhydrous diamond type δ-KYb_3F_{10} becomes mainly the cubic α-KYb_3F_{10} form, with an additional amount of YbF_3. By comparison with $(H_3O)Yb_3F_{10},H_2O$, the decomposition occurs at a higher temperature (+143°C). Similarly, the loss of zeolithic water between 150 and 250°C is also observed at higher temperature (this phenomenon was achieved at 130°C for the zeolithic water of $(H_3O)Yb_3F_{10},H_2O$). This difference may be due to the presence of the K^+ ions in the center of the windows of the cages, which probably produce a more difficult desorption of the water molecules through the tunnels.

It is noticeable that the infrared spectra exhibit the same bands (1630 and 3400–3600 cm^{-1}) as in the case of $(H_3O)Yb_3F_{10},H_2O$. However the observed bands are less broad, in agreement with the absence of the vibration modes of H_3O^+.

CONCLUSION

The original phase $(H_3O)Yb_3F_{10},H_2O$ has been synthesized at low temperature by a "chimie douce" route. The

TABLE 6
Atomic Parameters and Isotropic Beq Temperature Factors ($Å^2$) for δ-Yb_3F_{10},H_2O ($Fd\bar{3}m$, Origin: 16*c*)

Atom	Site	*x*	*y*	*z*	Beq
Yb	48*f*	$\frac{3}{8}$	$\frac{3}{8}$	0.0530(1)	0.93(1)
F_1	96*h*	0	0.8761(3)	−0.8761(3)	0.94(9)
F_2	32*e*	0.2131(3)	0.2131(3)	0.2131(3)	0.5*
F_3	32*e*	0.0524(3)	0.0524(3)	0.0524(3)	0.5*
K	16*d*	$\frac{1}{2}$	$\frac{1}{2}$	$\frac{1}{2}$	3.6(2)
H_2O	48*f*[a]	$\frac{3}{8}$	$\frac{3}{8}$	0.251(2)	3.1*

[a] Occupation ratio $\frac{1}{3}$.
* denotes fixed factor.

TABLE 7
Main Distances (Å) in δ-KYb_3F_{10},H_2O

Yb^{3+} polyhedron: [8]	F–F distances in the square antiprisms
$4\times Yb–F_1: 2.204(5)$	$2\times F_1–F_1 = 2.687(5)$
$2\times Yb–F_3: 2.258(5)$	$2\times F_1–F_1 = 2.736(5)$
$2\times Yb–F_2: 2.357(5)$	$4\times F_1–F_2 = 2.877(5)$
$\langle d_{Yb–F}\rangle = 2.26(1)$ Å	$4\times F_1–F_3 = 3.027(9)$
$d_{Shannon} = 2.28$ Å	$4\times F_2–F_3 = 2.487(7)$
Center of the hexagonal cavity	
$6\times K–F_1: 2.736(4)$	
Zeolithic water	
$4\times(H_2O)–F_1: 2.73(1)$	

synthesis of isotypic compounds of the lanthanide series is now in progress. A neutralization also allowed for the synthesis of δ-KYb_3F_{10},H_2O which is a new compound of the KYb_3F_{10} family.

These two structures have been described in a simple fashion based on the stacking of groups of six antiprisms, connected by edges around a cubic cavity, and defined as an Yb_6F_{32} $UOA_{[8]}$. The Yb_6F_{20} three-dimensional network corresponds to a diamond stacking of $UOA_{[8]}$ connected by vertices. The counterions (H_3O^+, K^+) are located at the center of the faces delimiting the cages of the structure. The zeolithic character of the water molecules is related to their mobility through the tunnels of this diamond structure.

The greatest interest of this work is to provide a very simplifying structural description based on the modes of connection between polyhedra instead of a complex one. In fact, the scale of the basic unit of description has grown from an atom or a polyhedron to a group of polyhedra. From this observation, the members of the KYb_3F_{10} family and several structures based on antiprism have also been reconsidered. The results of this study are reported in the following publication.

REFERENCES

1. D. D. Ikrami, N. I. Kuznetsova, V. S. Sidorov, and E. D. Ruchkin, *Russian J. Inorg. Chem.* **29,** 1350 (1984).
2. A. Boireau, B. Darriet, J. Grannec, P. Gravereau, N. Ruchaud, A. Tressaud, and F. Weill, IVth European Conference on Solid State Chemsitry, C41, Dresden (1992).
3. P. E. Werner, L. Eriksson, and M. Westdhal, *J. Appl. Crystallogr.* **18,** 367 (1985).
4. J. Laugier and A. Filhol, program CELREF (1978).
5. J. Rodriguez-Carvajal, program Fullprof, Version 2.6.1 (1994).
6. G. M. Sheldrick, "Shelxs-86 Program User Guide," Univ. of Göttingen (1986).
7. A. J. C. Wilson (Ed.), "International Tables for Crystallography," Vol. C. Kluwer Academic, Dordrecht (1992).
8. P. A. Stadelman, *Ultramicroscopy* **2,** 131 (1987).
9. S. Aléonard, J. C. Guitel, Y. Le Fur, and M. T. Roux, *Acta Crystallogr. B* **32,** 3227 (1976).
10. M. Labeau, S. Aléonard, A. Védrine, R. Boutonnet, and J. C. Cousseins, *Mater. Res. Bull.* **9,** 615 (1974).
11. V. Simonov and B. V. Butvesky, *Acta Crystallogr. B* **34,** 355 (1978).